Oxygen Field Dynamics in Bioconvection and the Spatial Organization of Multispecies Aerobic Bacteria

Oscar Gallardo-Navarro [1,*] Rinat Arbel-Goren [1,*] Bareket Dassa [2] Elias August [3] and Joel Stavans [1,†]

[1]Department of Physics of Complex Systems, Weizmann Institute of Science, Rehovot 7610001, Israel
[2]Department of Life Sciences Core Facilities, Weizmann Institute of Science, Rehovot 7610001, Israel
[3]Department of Engineering, Reykjavik University, Reykjavik, Iceland

(Received 14 April 2026; accepted 20 July 2026; published 19 August 2026)

Emergent self-organization is a hallmark of natural bacterial communities, whose spatial structures and dynamic gradients are shaped by the complex interplay among bacterial diversity, oxygen and its consumption, and motility and by hydrodynamic flows. Key aspects of the interplay between oxygen gradients and bacterial community spatial structure remain obscure. Here we aim to elucidate the role that oxygen plays in the self-organization of multispecies bacteria in the water column, focusing on oxytactic bioconvection suspensions of naturally coexisting aerobic bacteria and on self-organization near air-water interfaces. Combining microscopy, mapping of the oxygen field and controlled external oxygen levels, we show that species-specific oxygen affinities and consumption rates induce the formation of distinct bacterial layers near air-water interfaces, resulting in dynamic segregation during multispecies bioconvection, and play a key role in determining the nature of bioconvective patterns in single species suspensions. We further find that oxygen and bacterial fields are tightly coupled and fluctuate with similar spatiotemporal scales, giving rise to oxygen advection and a well-defined oxic-anoxic boundary. Together, our results illuminate the fundamental role that oxygen gradients play in multispecies bacterial active matter and its spatial self-organization, with implications for the formation and stability of ecological niches in aquatic and sedimentary environments.

DOI: 10.1103/n3ls-7ssf

I. INTRODUCTION

The appearance of oxygen on Earth following the Great Oxygenation Event circa 2.4 Gya ago, and its gradual rise to modern levels [1,2] brought profound changes on extant life and its organization. Oxygen enabled the efficient utilization of carbon sources during aerobic cellular respiration [3]. Motility along oxygen gradients (oxytaxis or aerotaxis) allowed bacterial cells to escape anaerobic growth-limiting conditions, providing cells with an important survival strategy [4]. In suspension, motile aerobic bacteria accumulate near the air-water interface to supply their metabolic needs for oxygen. Since the bacterial interior is denser than the surrounding medium by ∼10% [5,6], bacterial accumulation leads to a heavy layer that becomes gravitationally unstable above a threshold, set by a critical value of the Rayleigh number (Ra_c),

$$\mathrm{Ra} = \frac{\Delta\rho g}{\mu D} h^3, \tag{1}$$

where $\Delta\rho$ is the difference in density between the enriched bacterial layer and the medium, g is the gravitational acceleration, μ is the viscosity, D is a bacterial diffusion coefficient, and h is the suspension height. The collapse of this layer by a Rayleigh-Taylor instability leads to the formation of plumes [7–14], and the large-scale auto-organization of bacterial motion into collective flows known as bioconvection [6,15]. The coherent structures of these flows are characterized by scales that are larger than individual cells by about three orders of magnitude. Bioconvection is thus a prime example of active matter systems, together with bird flocks and fish schools. It occurs naturally in lakes [16,17] and tide pools [18], where organisms can leverage bioconvection for ecophysiological benefits [17].

Recent experiments with natural isolates of cohabiting aerobic bacteria have revealed that oxytactic bioconvection pattern characteristics are species specific [19]. Differences in cell morphology, motility characteristics and flagellar distribution could only account partially for pattern differences between species. However, other factors such as oxygen consumption and preference may play a key role in bridging the gap between scales in bioconvection.

In nature, bacteria live in complex, diverse ecological communities, many of which exhibit spatial self-organized structures and gradients, from microbial mats and soil [20] to the ocean and freshwater column of lakes and rivers [21]. Oxygen constrains the spatial organization of these communities, allowing different species to coexist. Bioconvection experiments with multispecies suspensions showed that bacteria of different species can undergo dynamically induced spatial segregation (DISS) [19], despite enhanced mixing by

*These authors contributed equally to this work.
†Contact author: joel.stavans@weizmann.ac.il

hydrodynamic flows [22]. The different species segregated into nested domains, with different space-locked regions exhibiting characteristics of the patterns of the individual strains. Importantly, DISS was only observed under conditions of bioconvection and was more marked when bacterial cell speed differences between strains were large.

Much of the understanding of bioconvection has been predicated on the assumption of a vertical oxygen gradient that bacteria can follow by oxytaxis. However, oxygen can be advected, mixed, and consumed, resulting in an oxygen field that may deviate from a simple vertical gradient. Theoretical studies based on hydrodynamic approaches suggest a coupling between the oxygen, bacterial concentration and velocity fields [7,8,11,12,23,24]. Despite extensive experimental work on oxytactic bioconvection [5,14,25–28], the oxygen field and its coupling to local bacterial concentrations remains to be experimentally elucidated. What is the mechanism and specific role that oxygen plays in determining species-specific oxytaxis-driven bioconvective patterns and segregation in multispecies bioconvection [19]?

Here we characterize experimentally the dynamics of oxygen in bioconvective flows and its effects on the spatial organization of multispecies oxytactic bacteria collected from the pristine communities of the Cuatro Ciénegas Basin (CCB), Mexico [29–31]. The shared ecological origin of the aerobic bacteria we chose from our library, sampled from the first two millimeters of microbial mats [32,33], allows us to combine them and follow a bottom-up approach in a multispecies context. Our experiments reveal that the oxygen concentration field is highly inhomogeneous despite enhanced mixing by the hydrodynamic flow and strongly coupled to the bacterial concentration field. Furthermore, bioconvective plumes constitute an important mechanism for the advection of oxygen and, together with bacterial consumption, support the creation of highly anoxic regions in suspensions. Last, we present evidence supporting the notion that species-dependent affinities for particular oxygen concentrations along a direction perpendicular to the air-liquid interface are crucial in understanding mechanistically species-specific bioconvective pattern characteristics, as well as spatial segregation.

II. RESULTS

A. Oxygen concentration fields across bioconvecting patterns

To study the oxygen field across the horizontal plane of bioconvective patterns and how this field differs among species, we followed the dynamics of bioconvection in suspensions of four motile aerobic species, as well as an aerobic nonmotile one as a control. Bacterial doubling times are larger than the duration of the experimental runs, so bacterial density did not change appreciably [19]. Representative steady-state bioconvective patterns in Fig. 1(a) (and Movie S1 in the Supplemental Material [34]) show that each species displayed different pattern characteristics. In these patterns, darker regions represent high bacterial density. Snapshots of the oxygen concentration fields at the bottom of the bioconvective suspensions, at different times are shown in Fig. 1(b) and Movie S2 in the Supplemental Material [34]. Below the bioconvection onset $\mathrm{Ra} < \mathrm{Ra}_c$ (0 min), the oxygen field was nearly homogeneous. Above the onset $\mathrm{Ra} > \mathrm{Ra}_c$ (∼8 min), marked gradients developed in the oxygen field across wells. While oxygen levels were high for *Exiguobacterium* sp.—and to a lesser extent for *B. pumilus*—(after 30 min), they were comparably low for the other species. However, oxygen levels at the bottom also became low for *Exiguobacterium* sp. suspensions of larger depths (Fig. S1 in the Supplemental Material [34]). Of note, the spatial fluctuation characteristics of the patterned bacterial and oxygen concentration fields, in particular those of *Exiguobacterium* sp. and *B. pumilus*, show similar features (see Movies S1 and S2 in the Supplemental Material [34]). In contrast, the nonmotile *Citrococcus* sp. exhibits no spatially fluctuating patterns, reflecting its sinking dynamics as it consumes oxygen.

B. Modulating air oxygen concentration above bioconvecting single-species suspensions

To obtain more insights into the role of oxygen as a driver of oxytactic bioconvection and in setting spatial pattern characteristics, we modulated the oxygen concentration in the air above bioconvecting suspensions of the different species in a steplike fashion and followed the effects on pattern dynamics. In Fig. 2(a) the oxygen concentration above suspensions is plotted as a function of time, and in Fig. 2(b) representative top views of the bioconvective patterns are shown for different oxygen concentrations (see Movie S3 in the Supplemental Material [34]). Reduction of the oxygen concentration to low-enough levels (∼2%) reduced bioconvection in all the suspensions, though it was significantly maintained at a low level in the case of *Exiguobacterium* sp. At ∼0.3%, bioconvection was nearly abolished in all suspensions. Remarkably, gradual increase of the oxygen levels revealed that bioconvection was reestablished in all species at oxygen concentrations (∼4% and ∼6% for *B. pumilus*) that are significantly smaller than ∼21%, the atmospheric oxygen level. However, bioconvective pattern characteristics differed from those before oxygen step down, as illustrated by the presence of more focused plumes. When oxygen levels returned to the atmospheric value, patterns recovered their characteristics [e.g., compare first and last images, Fig. 2(b) and Movie S3]. Note that patterns at the latest times appeared darker due to cell division. An important feature of patterns with reduced oxygen concentrations observed in Fig. 2(b) is that bioconvection becomes more confined to the central region of a well, whereas the regions near the rims exhibit little or altered bioconvection. While inward radial flows are observed at low oxygen concentrations after bioconvection is reestablished, outward radial flows appear after the steplike increases in oxygen concentration.

C. Coupling between the oxygen and bacterial concentration fields during bioconvection

The results in Fig. 1 show the inhomogeneous nature of the oxygen field at pattern scales, raising the question of whether the oxygen and bacterial concentration fields are independent or coupled across patterns. To follow simultaneously the oxygen and the bacterial concentration fields and study their correlation over time, we used a fiber optic probe to monitor locally the oxygen field at a given depth in the suspension

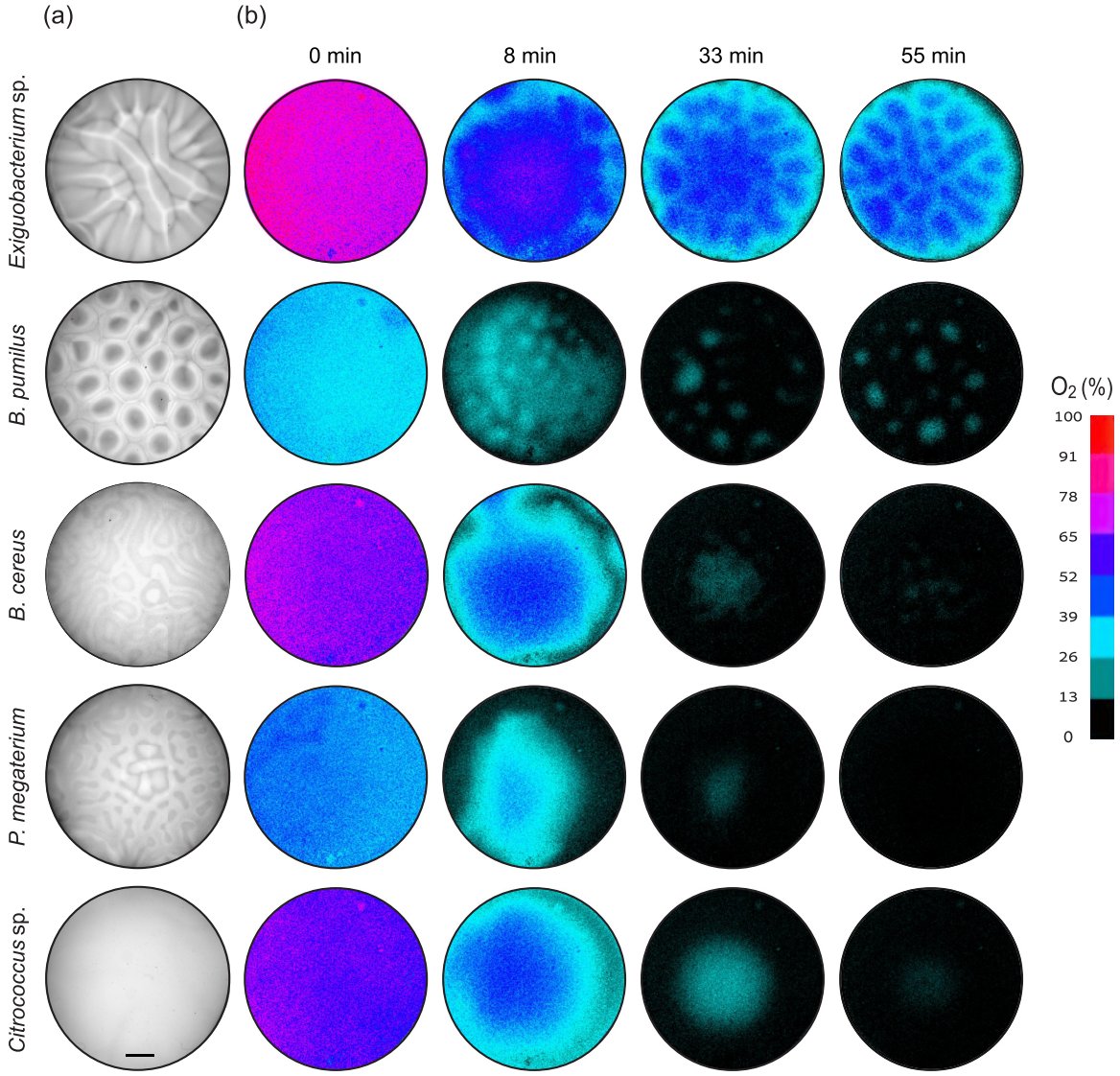

FIG. 1. Oxygen concentration field at the bottom of single-species bacterial suspensions undergoing bioconvection. (a) Representative steady-state bioconvective patterns of the indicated species observed by transmitted light stereomicroscopy from the top, about 55 min after the bioconvective onset (see Movie S1 in the Supplemental Material [34] for the dynamics of pattern formation). (b) Oxygen concentration as a function of time across bioconvective patterns, measured at the bottom of wells with oxygen-sensitive optodes. The color code in the right bar indicates the percentage of oxygen relative to its saturation in marine medium (see Movie S2 in the Supplemental Material [34] for the dynamics). Scale bar: 2 mm.

and the bacterial concentration near the probe. A region of the bioconvective pattern of *B. pumilus*, together with the fiber probe to measure the local oxygen concentration, are shown in Fig. 3(a) and Movie S4 in the Supplemental Material [34]. Mean transmitted light intensity in a small circular region was used as a measure of the mean local bacterial concentration. Both the oxygen and bacterial concentration display large fluctuations that have similar timescales and behavior [Fig. 3(b)] [34].

D. Transversal measurements of the oxygen field during bioconvection

The variation in oxygen concentration at the bottom of bioconvective suspensions of different species and heights (Figs. 1(b) and S1 in the Supplemental Material [34]), suggest that oxygen levels in a suspension depend strongly on depth. To study oxygen levels as a function of depth, we followed bioconvection from the side in vertical Hele-Shaw cells and used optodes as well as local probes to map the oxygen field.

Side visualization of bioconvection in suspensions of different species revealed that the unstable bacterial-rich layer near the top decays by down-welling plumes (Fig. 4 and Movie S5 in the Supplemental Material [34]), similarly to those observed previously for *B. subtilis* and in numerical studies [7,8,13,14,35]. Visualization reveals that the bacteria-depleted layer at the bottom of the Hele-Shaw cell also becomes buoyantly unstable to inverse, up-welling plumes. Importantly, both ordinary and inverse plumes are emitted not only during the initial instability when bioconvection sets in but also during steady states and hence are persistent features of the flow (Movie S5 in the Supplemental Material [34]). The

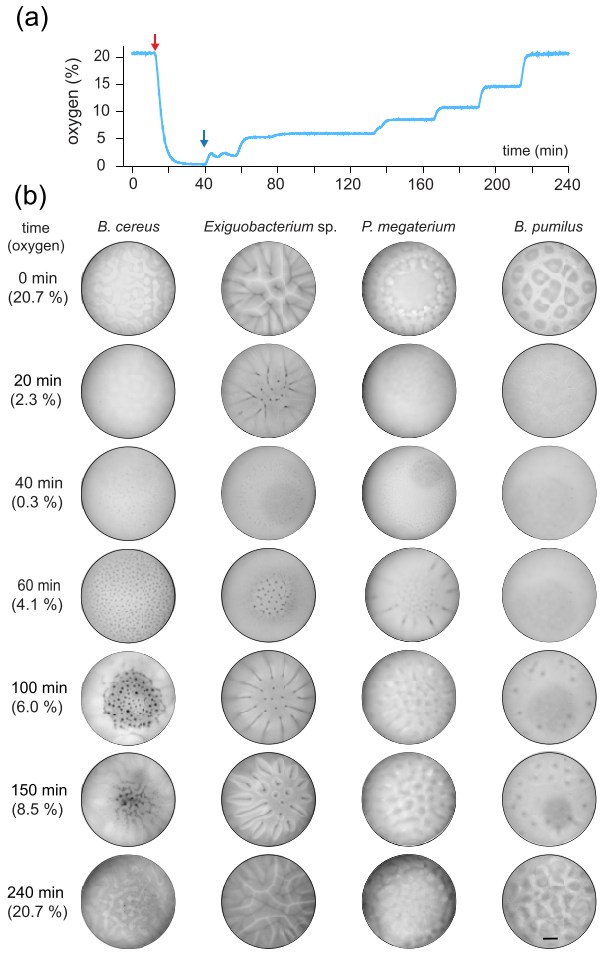

FIG. 2. Response of bioconvective patterns to changes in the oxygen concentration above a bacterial suspension. (a) Oxygen concentration in the air above bioconvecting suspensions of four different species [see (b)] was first reduced and then increased in a steplike fashion, allowing the bioconvective patterns to reach a steady state after each step. The red arrow indicates the time at which oxygen was initially reduced, and the blue arrow the time at which oxygen was reintroduced. Changes in oxygen were effected by flushing the chamber containing the suspensions with mixtures of atmospheric air and nitrogen. (b) Snapshots of bioconvective patterns in suspensions of the indicated species and times, carried out as in Fig. 1(a). Scale bar in the lower right panel represents 2 mm. See Movie S3 in the Supplemental Material [34] for the dynamics.

mean plume speeds for the different species were found to be comparable (Table I) and about twofold larger than the respective bacterial mean speeds [19], underscoring the important role of gravity in determining the dynamics of bioconvective flows. A theoretical prediction suggests that the transversal plume stem size scales as $\sqrt{\lambda}$, where λ is the thickness of the unstable layer that decays into a plume [13]. However, a plot of stem size at early times as a function of unstable layer thickness is more consistent with a linear dependence between these two quantities (Figs. S3(a) and S3(b) in the Supplemental Material [34]).

An important feature observed in Fig. 4(a) is a dark region of bacterial depletion around plume stems, whose width decreases from the top towards the bacteria-rich plume head. One may surmise that this depletion may be due to horizontal migration of bacteria towards plume stems, under the premise that plumes advect oxygen as they fall, as previously hypothesized [13]. To test this directly, we visualized the oxygen field from the side using optodes. Representative pictures of the oxygen field for single-species suspensions are shown in Fig. 4(b) (see also Movie S6 in the Supplemental Material [34]). At time zero, when the suspension is well mixed, the distribution of oxygen is nearly homogeneous. After 5 min, plumes develop in the top region simultaneously with an anoxic region at the bottom.

The plumes advect oxygen into the suspension, which is rapidly consumed within them before reaching the bottom, creating well-defined gradients within the plumes. Next we calculated the average oxygen concentration across horizontal sections to determine mean oxygen profiles as a function of depth for the different species. In a nearly well-mixed suspension [$t = 0$ min, Fig. 4(c)], the oxygen concentration falls to a species-dependent plateau value. Following the onset of bioconvection $\mathrm{Ra} > \mathrm{Ra}_c$ [$t \geqslant 5$ min, Fig. 4(d)], the plateaus decrease significantly for all species to the lowest oxygen levels, within a depth of ~2 mm. Complementary measurements using a fiber optic probe showed that oxygen levels were reduced from ~8 mg/l near the interface (100%), to about 0.6 mg/l (~7.5%) at a 2 mm depth for all species (Fig. S2 in the Supplemental Material [34]).

We next studied the effects of varying oxygen levels in the air on the behavior of plumes. Reduction of oxygen concentration brings about narrower plumes and differences in bioconvective behavior, consistent with observations in wells (Figs. S3(c) and S3(d) and Movie S7 in the Supplemental Material [34]). The width of the bacterial-rich layer near the interface λ increases monotonically with oxygen concentration (Fig. S3(d) in the Supplemental Material [34]).

E. The effects of oxygen concentration changes above bioconvecting multispecies suspensions

To test for the robustness of DISS to changes in oxygen concentration above multispecies bioconvective suspension, a binary suspension consisting of fluorescently labeled *Exiguobacterium* sp. and *P. megaterium* exhibiting segregation was subjected to steplike changes in the oxygen concentration [Fig. 5(a)]. At atmospheric oxygen levels (~21%), patterns display segregation (Fig. 5(b), Movie S8 in the Supplemental Material [34]). However, after oxygen step-down to ~0.19%, segregation is reduced concomitantly with bioconvection. At oxygen levels below ~2.4%, bioconvective activity concentrated primarily in the well's central region, without significant segregation. At a higher oxygen concentration, ~3.7%, segregation is reestablished. Segregation is concomitant with bioconvection of both species and is observed at oxygen concentrations that are lower than atmospheric levels. Similarly to the bioconvective patterns of single species (Fig. 2), plumes are narrower and more focused and tend to appear in the central region of the well. Reduction of oxygen above other binary suspensions yield similar results (Movie S9 in the Supplemental Material [34]).

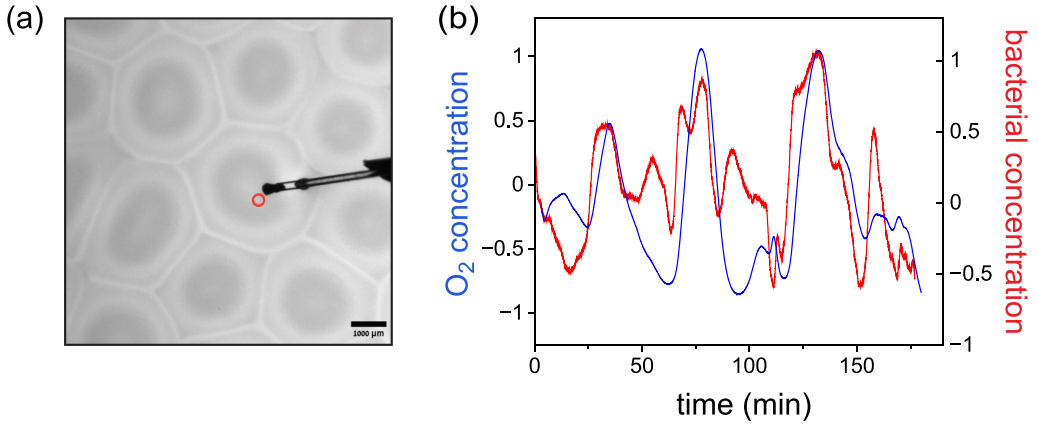

FIG. 3. Local oxygen and bacterial concentrations in a bioconvecting suspension. (a) Snapshot of a small region of a bioconvective pattern in an *Exiguobacterium* sp. suspension viewed from the top. Darker regions correspond to down-flowing current flows. The image also shows a fiber optic probe measuring the local oxygen concentration at its tip submerged at a given height, as well as a small circle (red) over which the intensity of transmitted light was averaged, as a measure of the local bacterial concentration near the probe tip. Scale bar: 1000 µm. (b) Normalized local measurements of oxygen (blue) and bacterial concentration (red) over time in a bioconvective pattern of an *Exiguobacterium* sp. suspension. For the dynamics see Movie S4 in the Supplemental Material [34].

F. Effects of oxygen concentration on bacterial band formation near air-liquid interfaces

In bioconvective patterns of multispecies suspensions displaying DISS, we observed that fast species were preferentially found down-flowing at the center of space-locked domains, surrounded by down-flowing regions rich in the slower species, e.g., when observing the faster *Exiguobacterium* sp. together with the slower *B. cereus* or *P. megaterium* [19]. We hypothesized that this feature may be due to preferential accumulation of the faster species near the air-liquid interface. To test this hypothesis, we quantified layer formation dynamics in suspensions near air-liquid interfaces in horizontal millifluidic channels [Fig. 6(a)], thereby eliminating the effects of gravitational instability. We also studied the effect of reducing the oxygen concentration in the air.

Remarkably, single species suspensions reached steady-state concentration profiles independently of their speed and displayed markedly different responses to oxygen gradients, forming bands at different distances away from the interface (Fig. 6(b) and Fig. S4 in the Supplemental Material [34]): Whereas *Exiguobacterium* sp. and *B. pumilus* migrated towards maximum oxygen concentrations at the interface as *B. subtilis* does [37], *B. cereus* and *P. megaterium* formed bands a distance away from the interface. These observations are quantified in Fig. 6(c), where we show concentration profiles as a function of distance from the interface.

Next, we carried out a bioinformatics analysis comparing key components in the oxytaxis network of the species used in this study to those of the Gram-positive *B. subtilis* strain 168. The analysis shows the presence of YfmS and HemAT-like oxygen sensor proteins, as well as details of the abundance of heme and chemotaxis-related protein families [38–40] in each bacterial species (see Fig. S5, Table SI and Supplemental Text in the Supplemental Material [34]).

We also studied band formation in multispecies suspensions. Experiments with selected binary suspensions exhibit the formation of two bands, with their positions determined largely by the intrinsic affinities of each species [Fig. 6(c)]. Moreover, the position of the band of a given species is moderately influenced by the presence of the other in the suspension. For instance, *B. cereus* is farther away from an interface when combined together with *Exiguobacterium* sp. However, its distribution is more tenuous and closer to the interface when present with *P. megaterium* [Fig. 6(d)].

Variation in the relative concentrations of species in a binary suspension of *Exiguobacterium* sp. and *B. cereus*, also affected their band positions (Fig. S6(a) in the Supplemental Material [34]). Increasing the relative abundance of *Exiguobacterium* sp., a species with a higher oxygen affinity, caused the *B. cereus* band to form farther away from the interface. Furthermore, a triple suspension consisting of *Exiguobacterium* sp., *B. cereus,* and *P. megaterium* also exhibited the formation of well-defined, separated bands (Fig. 6(e) and Fig. S6(b) in the Supplemental Material [34]). While the quantitative positions differed, their hierarchical position relative to the interface followed the order expected from experiments with single species [Fig. 6(b)–6(c)].

Finally, we studied species-specific band responses to reduced oxygen availability, by following the response of bacterial bands of different species [Fig. 7(a)]. Under steady-state conditions and atmospheric oxygen concentration, bands showed similar behavior as Figs. 6(b)–6(c). Reduction in oxygen resulted in band displacement towards the interface for *P. megaterium* and *B. cereus*, followed by dispersal, and only dispersal for *Exiguobacterium* sp. and *B. pumilus*, as the latter two already occupied the interface region.

III. DISCUSSION AND CONCLUSIONS

Despite advances in understanding bioconvection of oxytactic bacteria and its implications in both ecology and active matter physics, studies of the oxygen field driving it have been theoretical [6,25]. In the present study we have bridged this gap by mapping experimentally the oxygen field directly and establishing its coupling to local bacterial concentration. In addition, the results exposed the crucial role that species-

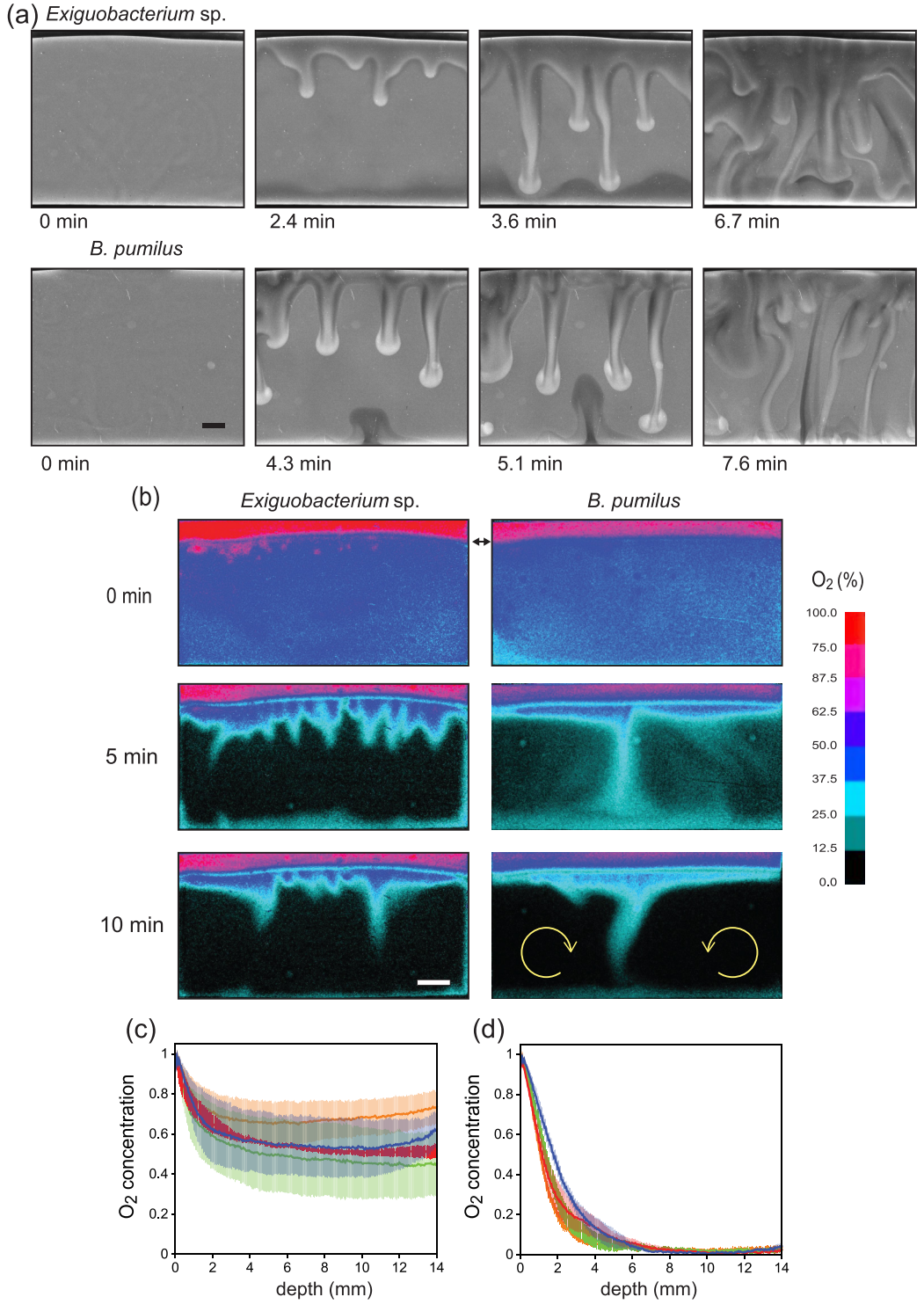

FIG. 4. Down-welling ordinary plumes and oxygen concentration dependence on depth in a Hele-Shaw cell. (a) Suspensions of *Exiguobacterium* sp. and *B. pumilus*, at different times above the bioconvective onset within vertical Hele-Shaw cells. The images were captured using transmitted light microscopy. Scale bar: 2 mm. See also Movie S5 in the Supplemental Material [34] for the dynamics, as well as for *P. megaterium* and *B. cereus*. (b) Representative snapshots of the normalized oxygen concentration at different times in suspensions of the same species. Time zero is defined when bioconvecting suspensions were injected to the Hele-Shaw devices. The color code shown in the right bar indicates the percentage of oxygen relative to its saturation in marine medium. The black double arrow indicates the air-liquid interface and the yellow arrows denote the bioconvective flow direction. Scale bar: 2 mm. See Movie S6 in the Supplemental Material [34] for the dynamics, as well as for *P. megaterium* and *B. cereus*. (c) Normalized mean oxygen concentration as a function of depth below the bioconvective onset of different bacterial species (*B. pumilus*, blue; *P. megaterium*, red; *B. cereus*, orange; and *Exiguobacterium sp.*, green). (d) Normalized mean oxygen concentration as a function of depth above the bioconvective onset for the same species as in (c). The curves represent means of three independent experiments and error bars represent standard errors.

TABLE I. Mean down-flowing plume and single-cell bacterial speeds. Plume speeds of the indicated strains were measured in Hele-Shaw cells, while single-cell mean bacterial speeds were computed from the distributions in Refs. [18,36].

Species	Plume speed (μm/s)	Bacterial speed (μm/s)
Exiguobacterium sp.	86 ± 7	31 ± 1
B. pumilus	74 ± 8	42 ± 2
P. megaterium	67 ± 1	16 ± 1
B. cereus	60 ± 7	25 ± 1

specific oxygen affinities and consumption play in setting bioconvective patterns, dynamical segregation and spatial ordering in a native multispecies context.

Far from varying solely as a vertical gradient, our bioconvection experiments show that the oxygen field fluctuates with timescales and length scales similar to those of local bacterial concentrations at distances sufficiently close to the air-water interface, confirming

its nature as a hydrodynamic field [7,8,11,12,23,24]. This is evident in the patterned oxygen fields at the bottom of wells bearing shallow suspensions of *Exiguobacterium* sp. and *B. pumilus*. The smaller levels of oxygen for *P. megaterium* and *B. cereus* is consistent with their higher oxygen consumption rates [19], indicating that downwelling flows in these suspensions transport oxygen towards the bottom less effectively.

We established a ∼2 mm deep, quasi-steady-state, sharp oxic-anoxic boundary, determined by the interplay among bacterial oxygen consumption, atmospheric oxygen diffusion, and flow. In natural settings, where aerobic and anaerobic species coexist, the formation and maintenance of anoxic zones is ecologically important as this creates niches for anaerobes to thrive [41]. The oxic-anoxic boundary we report is close in magnitude to that observed in microbial mats [42]. The fact that the bacteria in our study can still navigate in the highly anoxic region to sustain the bioconvective flow is consistent with a log-sensing strategy of oxygen gradients [37,43,44].

Plumes were observed not only during the Rayleigh-Taylor instability of both the bacteria-rich and bacteria-poor layers at the onset of bioconvection but also during steady states, showing that they are persistent coherent structures [45,46]. The fact that plume speeds are comparable between species and significantly larger than bacterial cell speeds, stresses the importance of gravity and buoyancy for bioconvection. Indeed, a Stokes flow estimate of the buoyant velocity scale $u \sim \frac{2\Delta\rho g r^2}{9\mu}$, where $r \sim 0.1$ cm is the typical radius of a plume head, and a density increase due to the presence of the bacteria $\Delta\rho \sim 10^{-5}$ g/cm^3 yields $u \sim 100$ μm/s, close to our measured values (Table I).

The measurements of the oxygen field in downwelling plumes, together with local probe measurements highlight the fluctuating nature of the oxygen field and its correlation with the bacterial concentration field at different depths. Down-flowing plumes emerge as the main mechanism for the transport of oxygen, bringing it into the suspension from the air-liquid interface and mixing it, while at the same time

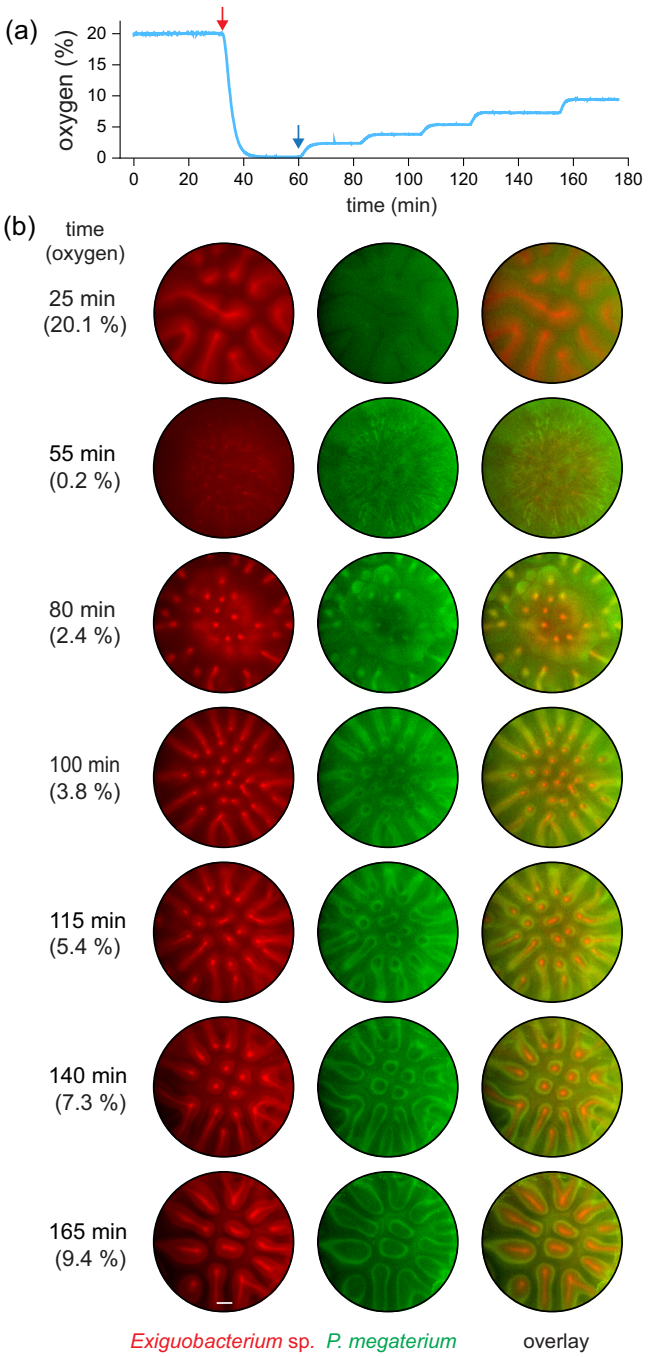

FIG. 5. Effects of changes in oxygen concentration above a bioconvective binary suspension on patterns displaying segregation. (a) Oxygen concentration in the air above a bacterial suspension undergoing bioconvection was first reduced and then increased in a steplike fashion, allowing bioconvective patterns in the suspension to reach a steady state after each step. The red arrow indicates the time of oxygen stepdown, the blue arrow the time at which oxygen was reintroduced and changes in oxygen were effected by flushing the chamber containing the suspension with mixtures of atmospheric air and nitrogen. (b) Representative stereomicroscopy images of bioconvective patterns in a binary suspension of fluorescently labeled *Exiguobacterium* sp. (red), *P. megaterium* (green), and overlay (third column) at a 1:1 volume ratio. See also Movies S8 and S9 in the Supplemental Material [34] for the dynamics. Scale bar: 1 mm.

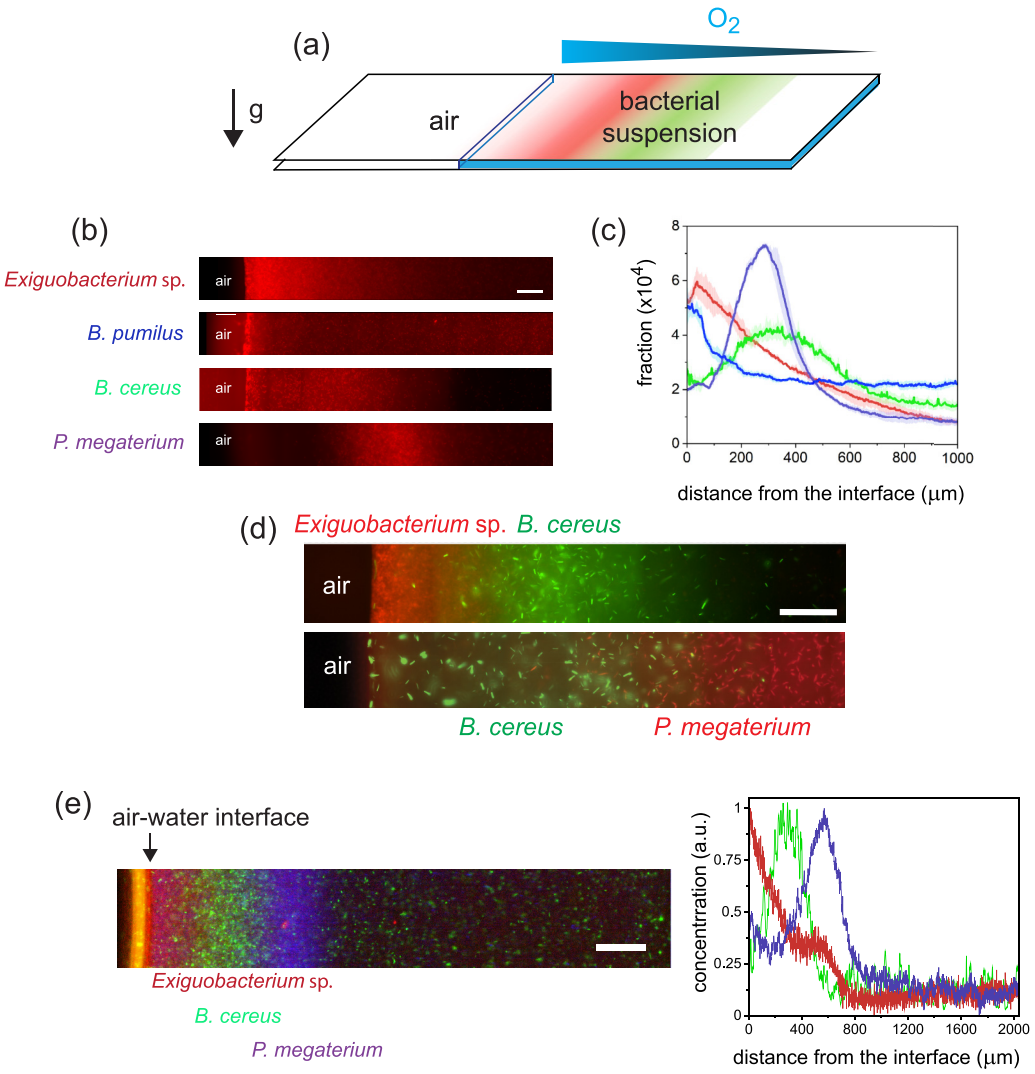

FIG. 6. Bacterial concentrations fields in horizontal channels with air-water interfaces. (a) Partially filled horizontal millifluidic channel containing single or multiple-species bacterial suspensions and an air-liquid interface. Oxygen gradients develop as a result of bacterial consumption. (b) Fluorescence microscopy images of band formation in single-species suspensions of surface-labelled bacteria (red) ∼30 min after introducing the suspensions into the channel. The bands shown represent a steady state. Scale bar: 100 μm. (c) Normalized mean concentration profiles of the different bacterial species in horizontal channels as in (b). Means were taken over three independent experiments for each species and error bars represent standard errors. (d) Fluorescence microscopy images of bands in two mixed binary bacterial suspensions: *Exiguobacterium* sp. and *P. megaterium* fluorescently labelled (red) and *B. cereus* (plasmid reporting GFP). Scale bar: 100 μm. (e) Stereomicroscopy images of bands in a triple suspension of *Exiguobacterium* sp. (red), *B. cereus* (green), and *P. megaterium* (violet), with relative volume ratios 2:1:1. Scale bar: 500 μm. The plot in the panel on the right represents the normalized fluorescence profile of the bands.

bacteria consume it. Indeed, a simple estimate suggests that diffusive transport is much slower: While it takes oxygen $\tau \sim \ell^2/D_O \sim 500$ s to diffuse across the transversal characteristic scale of a plume ($\ell \sim 0.1$ cm), assuming a diffusion coefficient of oxygen in water of $D_O \sim 2.1 \times 10^{-5}$ cm^2/s at 25 °C [47], the turnover time of a bioconvective roll of one millimeter height based on measured plume speeds is ∼10 times smaller. To dissect the roles of oxygen as a driving force behind bioconvection, we modulated the oxygen concentration in the air above suspensions. While bioconvection was nearly inhibited at near zero oxygen concentration levels, patterns with similar spatial characteristics were recovered when oxygen levels reached the atmospheric value. However, bioconvection started at oxygen well below the atmospheric value, suggesting again that the species we studied exhibit oxytactic responses consistent with a log-sensing strategy [37,43,44]. Spatial segregation in binary suspensions was also affected by variations of oxygen levels. As these decreased, convection cells progressively shrank until bioconvection was inhibited at near-zero oxygen concentrations. With a slight increase in oxygen concentration, bioconvection was restored; however, segregation did not reappear until higher oxygen levels were reached. We attribute this to changes in the oxygen gradient at the interface as the concentration declines. Specifi-

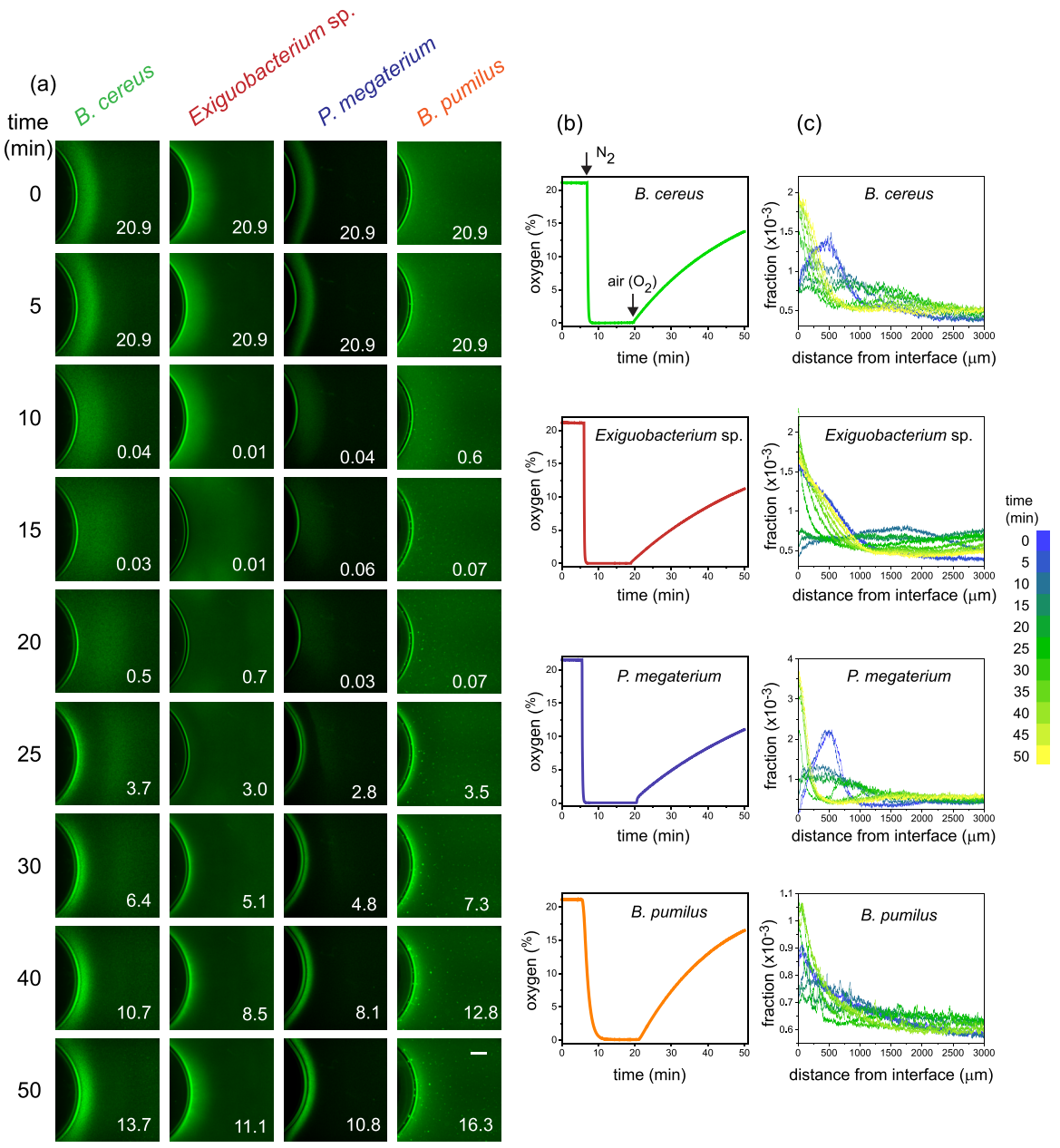

FIG. 7. Response of bands near an interface to modulation of oxygen concentration at the interface in horizontal suspensions. (a) Representative stereomicroscope snapshots of bacterial suspensions labeled with MitoTracker in horizontal channels at the indicated times, and their respective oxygen concentrations for each snapshot, following changes in the oxygen concentration at the interface (in v/v %) [see (b)]. The interface appears as a curved meniscus within the channel. Scale bar: 500 μm. (b) The oxygen concentration in the chamber was measured continuously as a function of time during the experiments as bands responded to oxygen changes. The suspensions, initially maintained in atmospheric air, were flushed with nitrogen gas (N_2 arrow), followed by gradual increase of oxygen concentration, carried out by allowing air to go into the chamber, about 10 min later (O_2 arrow). (c) Normalized fluorescence intensity as a function of distance from the interface for the snapshots shown in (a). The plots are color coded according to the bar (right) and the corresponding oxygen levels are determined in the plots in (b).

cally, the altered gradient drives the low-affinity species closer to the interface (Fig. 7), where it may disrupt segregation and accounts for the thinning of bioconvection plumes under low-oxygen conditions, as the bacterial layers become thinner when the cells accumulate nearer to the interface. Taken together, oxygen emerges as a key factor shaping bioconvective behavior, in suspensions of both single and multiple species. We cannot exclude that interactions mediated by resources and metabolites other than oxygen may also play a role. We note that DISS was observed under conditions where antagonistic interactions affecting mutual growth were not detected.

Species in horizontal channels showed distinct band dynamics in response to oxygen changes, each forming characteristic spatial profiles that reflect their specific oxygen preferences, consumption rates, and balance between respiration needs and toxicity avoidance [21]. Our bioinformatics

analysis shows that the species we studied differ considerably in their protein families. Yet they share Hem-like and Che-like protein families, known to be involved in oxygen sensing and chemotaxis in *B. subtilis* [48,49]. However, additional factors such as metabolism and oxygen consumption rates may play a role in accounting for differences in affinities and tolerance for oxygen.

The remarkable spatial segregation of species into bands observed in horizontal channels takes place within a fluid environment in which bacteria can move freely with no physical constraints, except for the oxygen gradients that the bacteria themselves help shape. It is thus fundamentally different from layering in proliferation patterns, in which bands form within gels without motility [50–53]. It is noteworthy that the segregation into bands occurred even when antagonistic biological interactions between the bacterial species were not detected. The segregation into distinct bands is most likely determined by species preferences for oxygen and relative bacterial concentrations. This auto-organization, within the oxic $\sim$1-mm-thick region adjacent to an air-water interface and observed in microcosms of natural bacterial isolates from CCB ponds [29], may have ecological implications and shed light on how multiple species of bacteria in the aerobic sector of microbial mats are organized.

Band formation and the ensuing segregation of species as function of the distance from an air-water interface suggests a unique mechanism that can underpin DISS, the segregation of species during multispecies bioconvection [19]. Band formation can make the layer of bacteria that eventually becomes buoyantly unstable through a Rayleigh-Taylor instability compositionally inhomogeneous: Species that migrate (Fig. S7(a) in the Supplemental Material [34]) towards a maximum oxygen concentration will be found near the interface, whereas those that are repelled from high oxygen concentrations will localize preferentially farther away (Fig. S7(b) in the Supplemental Material [34]). When this composite, inhomogeneous layer becomes unstable, species with high oxygen affinity will be found near the core of a plume, surrounded by those with lower affinity (Fig. S7(c) in the Supplemental Material [34]). While these latter can migrate horizontally by oxytaxis towards the oxygen-advecting plume, they will nonetheless remain at a distance from the core, given their aversion for high oxygen concentrations. Evidence in support of horizontal oxytactic migration is observed in bacterial depletion around plume stems [Fig. 4(a)]. Consistent with this picture, the oxygen consumption of *Exiguobacterium* sp. and *B. pumilus* is smaller than those of *P. megaterium* and *B. cereus*, and thus the plumes of the former species convey oxygen to larger depths. An additional contribution to inhomogeneity in the unstable layer can also come from large differences in motility between species, allowing faster species to reach the interface earlier. Coincidentally, *Exiguobacterium* sp. and *B. pumilus* both have larger speeds than *P. megaterium* and *B. cereus*. Importantly, the mechanism for segregation proposed above accounts for the observation that species with high affinity to oxygen concentrations and speeds are located at the center of space-locked convective domains, surrounded by the species with lower affinities and speeds [19]. The experimental observations reported here provide a basis for future theoretical studies aimed at supporting the mechanism behind differences in bioconvective patterns and DISS proposed here, e.g., by hydrodynamic approaches.

Layered microbial ecosystems such as phototrophic microbial mats and stromatolites [21,54–56] dominated aquatic and terrestrial habitats before the rise of multicellularity during the Cambrian explosion. Despite their sheer complexity, their basic structure is robust and has been proposed as a biosignature to test for life in other planets [57]. It is therefore notable that in the much simpler scheme of our experiments, different bacterial species segregate along an oxygen gradient, forming a well-defined layered structure. Our studies support the notion that this structure plays a crucial role in bioconvective phenomena, including the nature of patterns in individual species, as well as DISS in a multispecies setting.

Taken together, our results provide new insight into the dynamics of spatial self-organization in natural bacterial communities, particularly in layered systems such as microbial mats. They highlight the crucial role of mutual feedback between oxygen and bacterial fields in shaping spatial structure. Spatial structure emerges as a fundamental paradigm that cannot be neglected and represents a clear departure from the mean-field, well-mixed approaches that underpin many studies of microbial ecology [58].

Our experimental scheme paves the way for the controlled exploration of the fine-scale structure of the aerobic sector of microbial mats and its response to perturbations from a bottom-up perspective. For example, the response of bacterial bands to changes in oxygen illustrates how modulation of spatial organization can arise from circadian day-night oxygen cycles [21,55]. Extending this framework to include anaerobic species will open new opportunities to address mat complexity across scales, adaptation at oxic-anoxic interfaces, regime shifts [41], and the theoretical modelling of these systems [59,60].

ACKNOWLEDGMENTS

We thank Professor G. Olmedo-Alvarez for helpful discussions. We acknowledge support from the Minerva Stiftung with funding from the Federal German Ministry for Education and Research (to J.S.), a grant from the Weizmann SABRA-Yeda-Sela-WRC program, a Siegfried and Irma Ullman Professorial Chair (to J.S.), and Weizmann Institute of Science Visiting Faculty program supported by the Benoziyo Endowment Fund for the Advancement of Science (E.A.).

J.S. conceptualized and supervised the study; O.G.N., R.A.G., and J.S. developed the methodology; O.G.N., R.A.G., and J.S. carried out the investigation, visualization, and validation; O.G.N. carried out the experiments; O.G.N. R.A.G., E.A., and J.S. carried out analysis; B.D. carried out the bioinformatic analysis; J.S. and R.A.G. wrote the original draft while O.G.N., R.A.G., E.A., B.D., and J.S. reviewed and edited until the final version.

DATA AVAILABILITY

The data that support the findings of this article are openly available as specified in our manuscript.

APPENDIX: MATERIALS AND METHODS

1. Strains and culture conditions

Bacterial strains were isolated from superficial sediment at the margins of the oligotrophic Churince intermediate lagoon in the Cuatro Ciénegas Basin, Mexico [36]. Coordinates: 26.849142282661216, −102.14237282826757. See Table SII in the Supplemental Material [34] for list of strains. Bacterial stocks were stored in marine media with 15% v/v glycerol at −80 °C [61]. For the experiments, samples from the frozen stocks were streaked on marine media plates with 1.6% agar and incubated overnight at 28 °C. The next day, plates were placed at room temperature and used for up to 1 week. For the strain carrying the pNW-sfGFP plasmid, overnight liquid cultures of marine medium with chloramphenicol (10 μg/ml) were grown directly from the frozen stocks and incubated overnight at 28 °C and 250 rpm.

2. Sample preparation

A single colony was picked from a marine medium agar plate and incubated overnight in liquid marine medium at 28 °C and 250 rpm. The overnight culture was diluted to an OD_{600} of 0.7 (NanoDrop One C, ThermoFisher Scientific) in fresh marine medium. For *B. cereus*, 100 μl of the overnight culture was inoculated in 5 ml of fresh marine medium and incubated until reaching an OD_{600} of 0.7 to avoid the presence of cell aggregates that formed in overnight cultures. Vortexing and/or repeatedly aspiring and expelling the culture using a syringe was used to dissociate aggregates when needed. For bioconvection experiments, suspensions were placed either in circular wells (24-well Nunc Cell-Culture Treated Multidishes, Thermo Fisher Scientific) or in custom-made Hele-Shaw cells. The Hele-Shaw cells were made with two glass plates (50 × 25 × 1 mm) separated by a 2-mm rubber spacer, held together by a three-dimensionally (3D) printed scaffold. For experiments studying oxytactic behavior near air-liquid interfaces, millifluidic channel devices were used (μ-Slide VI 0.4 Bioinert, Ibidi). For fluorescence experiments, fluorescence dyes final concentrations were 3.2 μM for FM 4–64, 1 μM for MitoTracker Orange CMTMRos, 1 μM for MitoTracker Green FM (ThermoFischer Scientific), and 1 μM for MitoView 405 (Biotium). All dye stock solutions were prepared in dimethyl sulfoxide following manufacturer instructions. For mixed species experiments, single species were labelled separately, incubated for at least 5 min and mixed at the indicated volume ratios prior to loading into devices.

3. Sample visualization

Bioconvection dynamics in wells were recorded by taking 16-bit images with a fluorescence SMZ-25 stereomicroscope (Nikon) equipped with an Andor Zyla 4.2 Plus USB3 camera (Oxford Instruments), a SOLA Light Engine (Lumencor) and a motorized *x*-*y* stage (ProScan). Bioconvection was visualized from the top by placing a 400-μl volume (unless otherwise stated) of suspension in a well illuminated with transmitted light from the bottom, and therefore bacteria-rich regions appear dark by their absorbed light. For fluorescence visualization, the following filter sets were employed: 49008-ET mCherry filter set (Chroma Technology Corp.) for FM 4–64 and MitoTracker Orange CMTMRos; 49002-ET EGFP filter set (Chroma Technology Corp.) for MitoTracker Green FM and the constitutively expressed green fluorescent protein from pNW-sfGFP plasmid; and then 49028-ET DAPI filter set (Chroma Technology Corp.) for MitoView 405.

Bioconvection dynamics in vertical Hele-Shaw cells placed in the SMZ-25 stereomicroscope were recorded as indicated. The Hele-Shaw cells were obliquely illuminated by transmitted light, using a tilted mirror to redirect the image into the stereomicroscope's optical path. Bacteria-rich regions appear bright by their scattered light.

To characterize oxytactic behavior near air-liquid interfaces, fluorescently labelled samples from bioconvective suspensions were placed into millifluidic channels and transects of images were taken as a function of distance from the air-water interface. Images were then stitched together using the NIS-Element Advanced Research software (Nikon, version 5.02.01) to generate a long fluorescence image of the cell distribution along the transect at different timepoints. The setup consisted of an inverted microscope (Nikon, Ti2-Eclipse) with a motorized *x*-*y* stage (Prior). Stage, sample holder and objective (60 × /1.40 oil, Nikon) were inside a temperature box (Okolab) at 28 °C. Phase contrast and fluorescence images were acquired with a sensitive camera (Andor DU-987, X-4889). An experiment consisted of a sequence of images taken from a sample. Cells were illuminated with light of the appropriate wavelength, produced by a light emitting diode set (CoolLED pE-4000), using appropriate filter sets for each fluorescent dye: Chroma, 49002-ET-GFP (FITC/Cy2), for MitoTracker Green FM and Chroma, 49008-ET-mCherry, Texas Red, for FM 4–64 GFP. In some experiments, a single image was taken in the SMZ25 stereomicroscope.

4. Control of oxygen concentration in the air above suspensions

Mixtures of nitrogen and air were used to modify the air oxygen concentration inside a sealed well plate (24-well Nunc Cell-Culture Treated Multidishes, Thermo Fisher Scientific) at room temperature. Two holes were drilled on the lid of a Petri dish, one to insert a plastic tube connected to a gas mixer and the other to insert an optical oxygen microsensor (NTH-PSt7, PreSens). The plate-lid junction was sealed after placement of a bioconvection sample. Oxygen levels were continuously monitored in a neighboring well, while a bioconvection sample was imaged in the SMZ25 stereomicroscope.

5. Measurement of oxygen concentration

For measurements and visualization of the oxygen concentration field during bioconvection, a piece of oxygen-sensitive optode (SF-RPSu4, PreSens) was placed in either the inner side of one of the glass plates of the Hele-Shaw cell or in the bottom of a well. Time-lapse images were taken every 5 s with a camera designed to measure the optode signal (VisiSens, PreSens). A two-point calibration was performed at the beginning of each independent experiment by measuring a sample of sterile marine medium with and without 80 mM $NaSO_3$ as 0% and 100% oxygen saturation points, respectively. Process-

ing of the images was performed in the dedicated VisiSens ScientifiCal software to obtain the 2D oxygen fields.

Local oxygen measurements as a function of depth were done with an optical oxygen microsensor (NTH-PSt7, PreSens) mounted on a micrometric vertical stage over a Hele-Shaw cell at room temperature. The sensor was placed on the interface and lowered by fixed steps every 6 min. The first 2 min after each down step correspond to the stabilization period of the sensor and were not considered in the analysis. The remaining 4 min of the measurement were averaged to obtain the mean oxygen value for each step. At least two technical repetitions were averaged using interpolation to get the mean oxygen decay curve as a function of depth for a given independent experiment, and at least three independent experiments were conducted for each strain. The weighted average of all independent experiments was calculated to account for differences in number of technical repetitions. To measure the dynamics of the change in the oxygen concentration dissolved in the liquid, following changes in the oxygen concentration in the air above a suspension, the oxygen concentration was measured simultaneously in the air above a suspension in a closed 24-well plate using the optical oxygen microsensor and the dissolved oxygen concentration in the liquid using an optode at the bottom of a well (Fig. S8). About 20 min after a change in oxygen in the air suffice for the oxygen concentration in the liquid to nearly relax to its asymptotic value, in pure marine medium.

6. Image analysis of interface band profiles

Image analysis of stereomicroscope-acquired profiles was performed in MATLAB (Math-Works). RGB images were converted to grayscale. The surface meniscus was approximated as a circular arc, with its center and radius determined manually. A rectangular region corresponding to the water column was defined with its centerline passing through the meniscus center; the region had a width of 101 pixels (± 50 pixels) and was positioned to just contact the meniscus. Pixel intensity profiles were obtained by summing intensities across the width of the water column for each distance from the interface. Fluorescence profiles from microscope images were quantified using custom MATLAB code that summed pixel intensities per image row. The resulting profiles represent the bacterial concentration distribution, inferred from proportional fluorescence intensity.

7. Local oxygen measurements during bioconvection in a well

A volume of 2.5 ml of a bacterial suspension was placed in a six-well plate (Nunc Cell-Culture Treated Multidishes, Thermo Fisher Scientific) with a small hole on the lid covered with tape to allow access to optical oxygen microsensor (NTH-PSt7, PreSens). Visualization was performed by taking bright-field images every 2 s with a SMZ-25 stereomicroscope (Nikon). Oxygen measurement acquisition was performed with PreSens' software every 2 s, with a delay of 1 s with respect to image acquisition to avoid interference with the stereoscope's illumination. Image data was processed with the Fiji distribution of ImageJ [62] by measuring the mean pixel intensity of a circular region-of-interest of 30 pixels in diameter, near the oxygen sensor tip. This region-of-interest corresponds to the sensor's spatial resolution.

8. Analysis of plumes during bioconvection

For scaling analysis of plumes, images from movies of bioconvection for each species were chosen just before and after the onset of bioconvection for measurement of the boundary layer thickness and plume stem diameter, in the middle of the Hele-Shaw cell horizontally (Fig. S3 in the Supplemental Material [34]). Both quantities were measured manually using the *Measure Distance* tool of ImageViewer in MATLAB. For plume speed analysis, to each bioconvection movie an intensity threshold was applied for a good contrast between background and one to two plume heads, which were approximated by circles using *imfindcircles* in MATLAB. The speed was determined by the difference in circle-center-position from one frame to the other divided by the interframe interval time (2 s) and averaged over all frames. Note that the difference of plume-head-position between the first and the last frame divided by total time elapsed yielded virtually the same result.

9. Bacterial comparative genomics

Bacterial genomes and annotations were collected from The Bacterial and Viral Bioinformatics Resource Center (BV-BRC) [63] for *Bacillus pumilus* strain 145, *Bacillus cereus* strain CH111_4T and *Bacillus megaterium* strain CH447_14T (recently renamed to *Priestia megaterium* CH447_14T) and *Bacillus subtilis* strain 168 as a reference genome. Newly sequenced genomes for *Exiguobacterium* GOB958 (SRR32554000) and *Citrococcus zhacaiensis* 26a (SRX27907291) were assembled and annotated with the Comprehensive Genome Analysis Service. The bacterial phylogenetic tree was constructed with the Codon Tree pipeline at BV-BRC, with RAxML maximum likelihood model based on 352 single copy genes. To examine the conservation of protein families across bacterial genomes protein-coding genes in each bacteria were annotated and assigned into protein families based on their sequence conservation (PATRIC cross-genus PGfams), using the BV-BRC comparative systems pipeline. A comparison between the species was then summarized into a matrix of 8980 protein families and the results were visualized on a Hierarchically clustered heatmap. Sequence identity of the gene *hemAT* was estimated with BLASTP.

10. Statistics and reproducibility

Statistical analyses were performed using OriginPro 2023b and MATLAB R2022b. The images of bioconvective patterns shown in Figs. 1–3 and 5 are representative results from at least three independent experiments. Figure 4(a) shows representative results from at least three independent experiments, which were carried out in separate days. Figures 6 and 7 are representative results from at least three independent experiments, which were carried out in separate days. For other figures, reproducibility is indicated in their respective legends.

[1] H. D. Holland, The oxygenation of the atmosphere and oceans, Philos. Trans. R. Soc., B **361**, 903 (2006).

[2] T. W. Lyons, C. T. Reinhard, and N. J. Planavsky, The rise of oxygen in Earth's early ocean and atmosphere, Nature (Lond.) **506**, 307 (2014).

[3] P. G. Falkowski, T. Fenchel, and E. F. Delong, The microbial engines that drive earth's biogeochemical cycles, Science (New York, N.Y.) **320**, 1034 (2008).

[4] B. L. Taylor, I. B. Zhulin, and M. S. Johnson, Aerotaxis and other energy-sensing behavior in bacteria, Annu. Rev. Microbiol. **53**, 103 (1999).

[5] C. Dombrowski, L. Cisneros, S. Chatkaew, R. E. Goldstein, and J. O. Kessler, Self-concentration and large-scale coherence in bacterial dynamics, Phys. Rev. Lett. **93**, 098103 (2004).

[6] M. A. Bees, Advances in bioconvection, Annu Rev Fluid Mech **52**, 449 (2020).

[7] Y. Deleuze, C. Chiang, M. Thiriet, and T. Sheu, Numerical study of plume patterns in a chemotaxis–diffusion–convection coupling system, Comput. Fluids **126**, 58 (2016).

[8] A. Chertock, K. Fellner, A. Kurganov, A. Lorz, and P. A. Markowich, Sinking, merging and stationary plumes in a coupled chemotaxis-fluid model: A high-resolution numerical approach, J. Fluid Mech. **694**, 155 (2012).

[9] H. Yanaoka and T. Nishimura, Pattern wavelengths and transport characteristics in three-dimensional bioconvection generated by chemotactic bacteria, J. Fluid Mech. **952**, A13 (2022).

[10] I. M. Jánosi, J. O. Kessler, and V. K. Horváth, Onset of bioconvection in suspensions of *Bacillus subtilis*, Phys. Rev. E **58**, 4793 (1998).

[11] F. Ivančić, T. W. H. Sheu, and M. Solovchuk, Bacterial chemotaxis in thin fluid layers with free surface, Phys. Fluids **32**, 061902 (2020).

[12] A. J. Hillesdon, T. J. Pedley, and J. O. Kessler, The development of concentration gradients in a suspension of chemotactic bacteria, Bull. Math. Biol. **57**, 299 (1995).

[13] A. M. Metcalfe and T. J. Pedley, Falling plumes in bacterial bioconvection, J. Fluid Mech. **445**, 121 (2001).

[14] S. Liu, Q. Hou, D. Kearns, and Y. Wu, Self-organization of active plume lattice in bacterial bioconvection, Quant Biol **13**, e80 (2025).

[15] I. Aranson, Bacterial active matter, Rep. Prog. Phys. **85**, 076601 (2022).

[16] T. Sommer *et al.*, Bacteria-induced mixing in natural waters, Geophys. Res. Lett. **44**, 9424 (2017).

[17] F. Di Nezio, S. Roman, A. Buetti-Dinh, O. Sepúlveda Steiner, D. Bouffard, A. Sengupta, and N. Storelli, Motile bacteria leverage bioconvection for ecophysiological benefits in a natural aquatic environment, Front. Microbiol. **14**, 1253009 (2023).

[18] R. N. Bearon and D. Grünbaum, Bioconvection in a stratified environment: Experiments and theory, Phys. Fluids **18**, 127102 (2006).

[19] O. Gallardo-Navarro, R. Arbel-Goren, E. August, G. Olmedo-Alvarez, and J. Stavans, Dynamically induced spatial segregation in multispecies bacterial bioconvection, Nat. Commun. **16**, 950 (2025).

[20] I. Engelhardt, D. Patko, Y. Liu, M. Mimault, T. de Las Heras Martinez, G. George, M. MacDonald, M. Ptashnyk, T. Sukhodub, N. Stanley-Wall, and N. Holden, Novel form of collective movement by soil bacteria, ISME J. **16**, 2337 (2022).

[21] T. Fenchel and B. Finlay, Oxygen and the spatial structure of microbial communities, Biol. Rev. **83**, 553 (2008).

[22] A. Sokolov, R. E. Goldstein, F. I. Feldchtein, and I. S. Aranson, Enhanced mixing and spatial instability in concentrated bacterial suspensions, Phys. Rev. E **80**, 031903 (2009).

[23] A. J. Hillesdon and T. J. Pedley, Bioconvection in suspensions of oxytactic bacteria: Linear theory, J. Fluid Mech. **324**, 223 (1996).

[24] N. A. Hill and T. J. Pedley, Bioconvection, Fluid Dyn. Res. **37**, 1 (2005).

[25] I. Tuval, L. Cisneros, C. Dombrowski, C. W. Wolgemuth, J. O. Kessler, and R. E. Goldstein, Bacterial swimming and oxygen transport near contact lines, Proc. Natl. Acad. Sci. USA **102**, 2277 (2005).

[26] D. Shoup and T. Ursell, Bacterial bioconvection confers context-dependent growth benefits and is robust under varying metabolic and genetic conditions, J. Bacteriol. **205**, e00232 (2023).

[27] A. Czirok, I. M. Janosi, and J. O. Kessler, Bioconvective dynamics: Dependence on organism behaviour, J. Exp. Biol. **203**, 3345 (2000).

[28] I. M. Jánosi, A. Czirók, D. Silhavy, and A. Holczinger, *Jamming Bacterial Traffic: Bioconvection, in Traffic and Granular Flow'01* (Springer, Berlin, Heidelberg, 2003), pp. 569–574.

[29] V. Souza, G. Olmedo-Álvarez, and L. Eguiarte, *Cuatro Ciénegas Ecology, Natural History and Microbiology* (Springer, New York, 2018).

[30] M. D. R. Torres, L. D. Alcaraz, V. Souza, and G. Olmedo-Álvarez, Single genus approach to understanding bacterial diversity, niche, distribution, and genomics, in *Cuatro Ciénegas Ecology, Natural History and Microbiology* (Springer, Berlin, 2018), pp. 103–112.

[31] V. Souza, A. Moreno-Letelier, M. Travisano, L. David Alcaraz, G. Olmedo, and L. Enrique Eguiarte, The lost world of Cuatro Ciénegas Basin, a relictual bacterial niche in a desert oasis, eLife **7**, e38278 (2018).

[32] M. D. Rodríguez-Torres, Á. Islas-Robles, Z. Gómez-Lunar, L. Delaye, I. Hernández-González, V. Souza, M. Travisano, and G. Olmedo-Álvarez, Phenotypic microdiversity and phylogenetic signal analysis of traits related to social interaction in Bacillus spp. from sediment communities, Front. Microbiol. **8**, 29 (2017).

[33] E. A. Rebollar, M. Avitia, L. E. Eguiarte, A. González-González, L. Mora, G. Bonilla-Rosso, and V. Souza, Water–sediment niche differentiation in ancient marine lineages of Exiguobacterium endemic to the Cuatro Cienegas Basin, Environ. Microbiol. **14**, 2323 (2012).

[34] See Supplemental Material at http://link.aps.org/supplemental/10.1103/n3ls-7ssf for Figs. S1–S8, Tables SI and SII, movies S1–S9, additional text on bioinformatic analysis, which includes Refs. [19,36,38,39,40].

[35] H. G. Lee and J. Kim, Numerical investigation of falling bacterial plumes caused by bioconvection in a three-dimensional chamber, Eur. J. Mech. B. Fluids **52**, 120 (2015).

[36] R. A. Pérez-Gutiérrez *et al.*, Antagonism influences assembly of a Bacillus guild in a local community and is depicted as a food-chain network, ISME J. **7**, 487 (2013).

[37] F. Menolascina, R. Rusconi, V. I. Fernandez, S. Smriga, Z. Aminzare, E. D. Sontag, and R. Stocker, Logarithmic sensing

in Bacillus subtilis aerotaxis, npj Syst. Biol. Appl. **3**, 16036 (2017).

[38] K. D. Collins, J. Lacal, and K. M. Ottemann, Internal sense of direction: Sensing and signaling from cytoplasmic chemoreceptors, Microbiol. Mol. Biol. Rev. **78**, 672 (2014).

[39] W. Zhang and G. N. Phillips, Structure of the oxygen sensor in Bacillus subtilis: Signal transduction of chemotaxis by control of symmetry, Structure **11**, 1097 (2003).

[40] H. Yoshimura, S. Yoshioka, K. Kobayashi, T. Ohta, T. Uchida, M. Kubo, T. Kitagawa, and S. Aono, Specific hydrogen-bonding networks responsible for selective O_2 sensing of the oxygen sensor protein HemAT from Bacillus subtilis, Biochemistry **45**, 8301 (2006).

[41] A. Brune, P. Frenzel, and H. Cypionka, Life at the oxic–anoxic interface: Microbial activities and adaptations, FEMS Microbiol. Rev. **24**, 691 (2000).

[42] B. B. Jørgensen and D. J. Des Marais, The diffusive boundary layer of sediments: Oxygen microgradients over a microbial mat, Limnol. Oceanogr. **35**, 1343 (1990).

[43] M. Morse, R. Colin, L. G. Wilson, and J. X. Tang, The aerotactic response of caulobacter crescentus, Biophys. J. **110**, 2076 (2016).

[44] J. B. Kirkegaard, A. Bouillant, A. O. Marron, K. C. Leptos, and R. E. Goldstein, Aerotaxis in the closest relatives of animals, eLife **5**, e18109 (2016).

[45] G. Zocchi, E. Moses, and A. Libchaber, Coherent structures in turbulent convection, an experimental study, Physica A **166**, 387 (1990).

[46] D. Schmeling, J. Bosbach, and C. Wagner, Measurements of the dynamics of thermal plumes in turbulent mixed convection based on combined PIT and PIV, Exp. Fluids **56**, 134 (2015).

[47] R. T. Ferrell and D. M. Himmelblau, Diffusion coefficients of nitrogen and oxygen in water, J. Chem. Eng. Data **12**, 111 (1967).

[48] S. F. El-Mashtoly, Y. Gu, H. Yoshimura, S. Yoshioka, S. Aono, and T. Kitagawa, Protein conformation changes of HemAT-Bs upon ligand binding probed by ultraviolet resonance Raman spectroscopy, J. Biol. Chem. **283**, 6942 (2008).

[49] N. J. Hoque and E. E. Weinert, Control of bacterial second messenger signaling and motility by heme-based direct oxygen-sensing proteins, Curr. Opin. Genet. Dev. **76**, 102396 (2023).

[50] J. W. T. Wimpenny, Responses of microorganisms to physical and chemical gradients, Philos. Trans. R. Soc. Lond. Ser. B **297**, 497 (1982).

[51] J. W. T. Wimpenny and H. Abdollahi, Growth of mixed cultures of Paracoccus denitrificans and Desulfovibrio desulfuricans in homogeneous and in heterogeneous culture systems, Microb. Ecol. **22**, 1 (1991).

[52] J. P. Coombs and J. W. T. Wimpenny, Growth of Bacillus cereus in a gel-stabilized nutrient gradient system, Microbiology (N.Y.) **128**, 3093 (1982).

[53] J. S. Chuang, R. Rao, and S. Leibler, Bacterial proliferation pattern formation, PRX Life **3**, 013007 (2025).

[54] D. J. Des Marais, Microbial mats and the early evolution of life, Trends Ecol. E **5**, 140 (1990).

[55] J. Franks and J. Stolz, Flat laminated microbial mat communities, Earth Sci. Rev. **96**, 163 (2009).

[56] A. Gutiérrez-Preciado, A. Saghaï, D. Moreira, Y. Zivanovic, P. Deschamps, and P. López-García, Functional shifts in microbial mats recapitulate early Earth metabolic transitions, Nat. Ecol. E **2**, 1700 (2018).

[57] A. Goyal and M. Tikhonov, Energy-ordered resource stratification as an agnostic signature of life, Nat. Commun. **16**, 2867 (2025).

[58] M. Bäcker, H. M. Doekes, D. R. Garza, J. Meijer, S. van Vliet, R. J. Allen, P. Hogeweg, B. E. Dutilh, and B. van Dijk, Spatial structure: Shaping the ecology and evolution of microbial communities, FEMS Microbiol. Rev. **50**, fuaf067 (2026).

[59] T. Bush, M. Diao, R. J. Allen, R. Sinnige, G. Muyzer, and J. Huisman, Oxic-anoxic regime shifts mediated by feedbacks between biogeochemical processes and microbial community dynamics, Nat. Commun. **8**, 789 (2017).

[60] A. Goyal, A. Flamholz, A. Petroff, and A. Murugan, Closed ecosystems extract energy through self-organized nutrient cycles, Proc. Natl. Acad. Sci. USA **120**, e2309387120 (2023).

[61] Ó. A. Gallardo-Navarro and M. Santillán, Three-way interactions in an artificial community of bacterial strains directly isolated from the environment and their effect on the system population dynamics, Front. Microbiol. **10**, 2555 (2019).

[62] J. Schindelin *et al.*, Fiji: An open-source platform for biological-image analysis, Nat. Methods **9**, 676 (2012).

[63] R. D. Olson, R. Assaf, T. Brettin, N. Conrad, C. Cucinell, J. J. Davis, D. M. Dempsey, A. Dickerman, E. M. Dietrich, and R. W. Kenyon, Introducing the bacterial and viral bioinformatics resource center (BV-BRC): A resource combining PATRIC, IRD and ViPR, Nucleic Acids. Res. **51**, D678 (2023).